

First-Principles Modeling of Pt/LaAlO₃/SrTiO₃ Capacitors Under an External Bias Potential

Claudio Cazorla¹ and Massimiliano Stengel^{1,2}

¹*Institut de Ciència de Materials de Barcelona (ICMAB-CSIC), 08193 Bellaterra, Spain*

²*ICREA - Institució Catalana de Recerca i Estudis Avançats, 08010 Barcelona, Spain**

We study the electrical properties of Pt/LaAlO₃/SrTiO₃ capacitors under the action of an external bias potential, using first-principles simulations performed at constrained electric displacement field. A complete set of band diagrams, together with the relevant electrical characteristics (capacitance and *built-in* fields), are determined as a function of LaAlO₃ thickness and the applied potential. We find that the internal field in LaAlO₃ monotonically decreases with increasing thickness; hence, the occurrence of spontaneous Zener tunneling is ruled out in this system. We discuss the implications of our results in the light of recent experimental observations on biased LaAlO₃/SrTiO₃ junctions involving metallic top electrodes.

PACS numbers: 73.20.-r, 71.15.-m, 71.70.-d

In recent years oxide-oxide heterojunctions have generated widespread interest, because of their potential for applications in microelectronics and intriguing fundamental physics. When thin films of polar LaAlO₃ (LAO), composed of formally charged (LaO)⁺ and (AlO₂)⁻ layers, are stacked on top of the non-polar (001) surface of SrTiO₃ (STO), a two-dimensional metallic electron gas appears at the interface under suitable experimental conditions [1]. In particular, TiO₂-terminated LAO/STO interfaces are found to undergo an insulating-to-conducting transition (named “electronic reconstruction”) when the thickness of the LAO film exceeds 3 – 4 layers [2]. Alternatively, 2D metallicity can be switched on and off by applying an external bias potential between the conducting LAO/STO interface and a metallic electrode placed on top of the free LAO surface [3–8]. In the latter setup (i.e. an asymmetric capacitor where the bottom electrode is the 2D electron gas, see Fig. 1) novel striking phenomena have been observed recently, which hold promise for the realization of novel field-effect devices with high operation speed and low power consumption.

First, Singh-Bhalla *et al.* [7] reported a non-trivial dependence of the tunneling current on the LAO thickness, d_{LAO} , with an abrupt increase at $d_{\text{LAO}} = 20$ unit cells. This was ascribed to the presence of a *built-in* electric field, which would cause Zener breakdown in the LAO film after exceeding a certain d_{LAO} critical value. The electrical response of the tunnel junction also displayed a clear hysteretic behavior as a function of applied voltage, suggesting interesting opportunities for memory applications. Second, the measured capacitance was found to undergo a remarkable increase at low carrier densities [8]. This enhancement was ascribed to the peculiar electronic properties of the 2D electron gas at the LAO/STO interface, and in particular to a “negative compressibility” regime. While such a behavior was already known in the context of semiconductor heterojunctions, its unprecedented magnitude (40%) in the LAO/STO system challenges the current theoretical understanding of this effect.

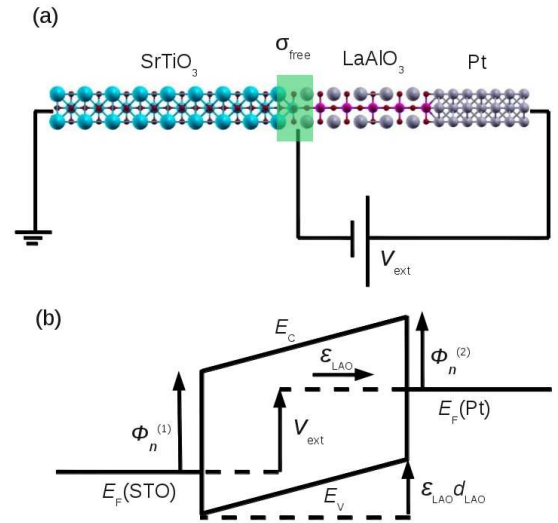


FIG. 1: (a) Schematic illustration of the Pt/LAO/STO capacitor; large blue spheres represent Sr atoms, small blue Ti, red O, large purple La, pink Al and small purple Pt. (b) Pt/LAO/STO band diagram; $\phi_n^{(1,2)}$ are the *n*-type SBH at the LAO/STO and Pt/LAO junctions, ϵ_{LAO} is the electric field in LAO, d_{LAO} is the thickness of the film, E_V / E_C are the valence / conduction band edges, E_F are the Fermi levels, and V_{ext} is the external bias potential.

Rationalizing these phenomena in terms of the microscopic properties of the LAO/STO and LAO/electrode junctions is very desirable in sight of future progress. In this context, first-principles electronic structure methods appear ideally suited to describing, with unbiased accuracy, the subtle interplay between carrier confinement, polar distortions and electrical perturbations applied to the sample. Indeed the LAO/STO system has been addressed by a large number of ab-initio studies in the past few years [9–16]. However, studying the phenomena described in Refs. [7] and [8] entails some additional technical challenges, because of the necessity of introducing

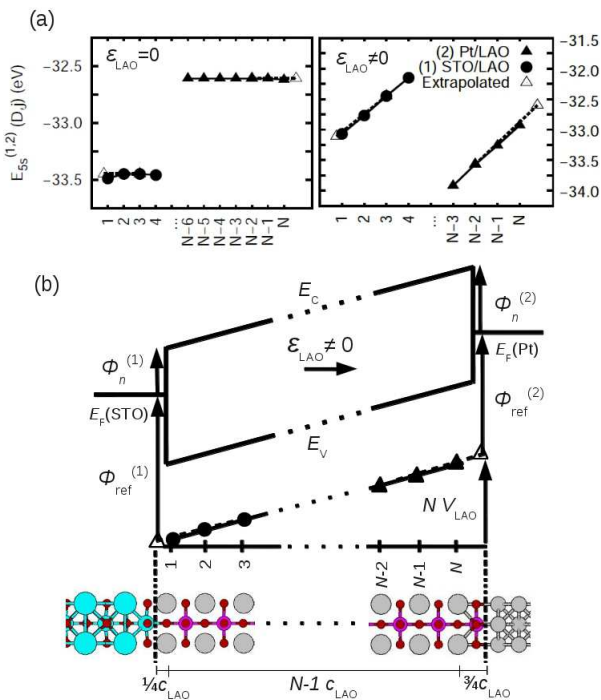


FIG. 2: (a) Layer-resolved La 5s semicore energies, $E_{5s}^{(1,2)}$, obtained at $D = -0.5 e/S$ (left) and $-0.3 e/S$ (right). Triangles represent the extrapolated values at the interfaces, $\phi_{\text{ref}}^{(1,2)}$. (b) Sketch of the Pt/LAO/STO band diagram and details of the extrapolation scheme (see text).

an external voltage in a complex capacitor system that is overall metallic.

In this Letter, we propose an elegant solution to this problem by using recently developed methods [17, 18] to perform *ab initio* simulations at constant electric displacement D . In particular, we show that: (i) the internal electric field (\mathcal{E}_{LAO}) in a Pt/LAO/STO capacitor is not an intrinsic and fixed quantity, but a function of both applied bias and LAO thickness; (ii) at zero bias, \mathcal{E}_{LAO} monotonically decreases with film thickness as $\sim 1/d_{\text{LAO}}$, so that no Zener breakdown ever occurs; (iii) the LAO/STO interface is associated with a capacitance, predominantly due to band bending effects, which is constant within a wide range of carrier densities. Based on these findings we deduce a complete set of *ab initio* band diagrams and a simple analytical expression for \mathcal{E}_{LAO} as a function of the relevant parameters. Finally, we discuss the implications of our results for the interpretation of experimental observations in [8] and [7].

To start with, we are interested in determining the electronic and structural properties of an arbitrarily thick Pt/LAO/STO capacitor subjected to an external bias potential V_{ext} . Instead of working directly at fixed V_{ext} , we use the electric displacement field D as independent electrical variable; this has clear advantages from the point of view of modeling [19], as it allows one to break down a

layered system into smaller constituents and treat them separately (“locality principle”). (Note that working at fixed V or at fixed D yields the exact same information, except that we express it in terms of two different macroscopic electrical variables; these are related by a Legendre transformation [17].) In our case, we shall consider the LAO/STO interface [(1) henceforth], bulk LAO and the Pt/LAO interface [(2) henceforth]. Following the arguments of Refs. [17] and [20], we can decompose the total potential drop V_{tot} across the capacitor into three terms (see Fig. 1),

$$V_{\text{tot}}(D, N) = \phi_n^{(1)}(D) - \phi_n^{(2)}(D) + N V_{\text{LAO}}(D). \quad (1)$$

Here $V_{\text{LAO}} = -\mathcal{E}_{\text{LAO}} c_{\text{LAO}}$ (c_{LAO} is the out-of-plane lattice parameter) is the potential drop across one unit cell of bulk LAO, N the number of unit cells, and $\phi_n^{(1,2)}$ are the (D -dependent) n -type Schottky barrier heights (SBH) at the metal/insulator junctions [17]. Note that to obtain the ground state of the system at a given applied potential V_{ext} one simply needs to invert Eq. (1) and solve for $V_{\text{tot}}(D, N) = V_{\text{ext}}$. This way, the daunting problem of simulating the full Pt/LAO/STO capacitor under an external bias reduces to the more familiar task of calculating SBH at metal/insulator interfaces as a function of D . As we shall explain in the following, it is relatively straightforward to do this with a standard first-principles code, without the need for a specialized finite-field (or even Berry-phase) implementation.

Our calculations are performed within the local density approximation of density functional theory and the PAW method [21], as implemented in the in-house code LAUTREC [22]. We compute the quantities on the right hand side of Eq. (1) by means of three separate calculations: two interface models within a X/LAO/vacuum slab geometry, where X is the metallic electrode (either Pt or STO), and a periodic LAO bulk model. For the X/LAO interfaces we use stacks of 10/7 (X=Pt) and 12/5 (X=STO) layers respectively. The in-plane periodicity is set to 1×1 perovskite cells, with the lattice parameter fixed to the theoretical equilibrium value of bulk STO ($a_{\text{STO}} = 3.85 \text{ \AA}$). To constrain the electric displacement to a given value we introduce a layer of bound charges Q at the free LAO surface via the virtual crystal approximation [23]. By applying a dipole correction in vacuum, we enforce $D = 0$ outside the free surfaces; then, provided that the surfaces remain locally insulating, we have $D = Q/S$ [18, 24]. We explore values of D within the range $-0.5 e/S \leq D_{\text{LAO}} \leq -0.3 e/S$ (D_{STO} is set to zero).

To extract the dependence of the SBH on D , we use computational techniques similar to those in Refs. [25] and [24]. In particular, for the estimation of the band offset $\phi_n^{(1,2)}(D)$ we need two independent quantities, the so-called *lineup* term (an interface property) and the *band-structure* term (a bulk property) [24]. The lineup term

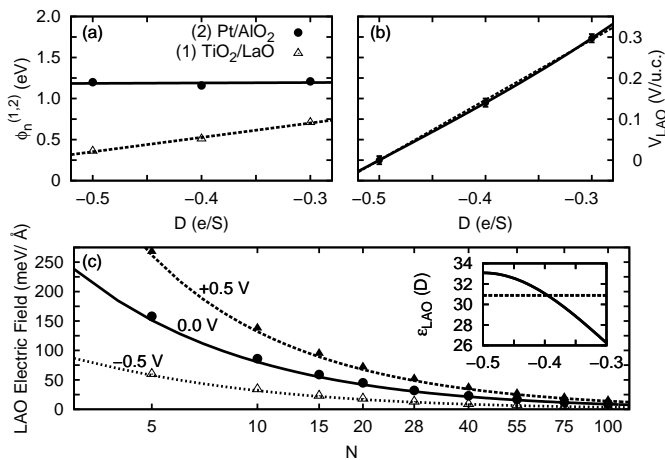


FIG. 3: (a) Calculated n -SBH as a function of D . The curves represent the linear fits $\phi_n^{(1)}(D) = 0.35 + 1.62(D + e/2S)$ and $\phi_n^{(2)}(D) = 1.18 + 0.05(D + e/2S)$ (in units of V). (b) Calculated potential drop per unit cell of bulk LAO; $V_{\text{LAO}}(D) = 1.27(D + e/2S) + 2.24(D + e/2S)^3$ (solid line) and $V_{\text{LAO}}(D) = 1.36(D + e/2S)$ (dashed line). (c) \mathcal{E}_{LAO} as a function of the number of LAO layers and bias potential $-0.5 \leq V_{\text{ext}} \leq 0.5$ V. The x -axis is in logarithmic scale. Symbols and lines represent results obtained with Eqs. (1) and (6), respectively. Inset: Static dielectric constant of bulk LAO as a function of DS/e (solid curve) and the corresponding averaged value $\bar{\epsilon}_{\text{LAO}}$ (dashed line).

relies on the choice of a reference energy in the insulating LAO layer; here we use the La 5s semicore energy, that we extract from the layer-resolved density of states of the slab models. We define as $E_{5s}^{(1,2)}(D, j)$ the energy location of the La 5s peak in the j -th LaO layer of the (1) or (2) system, referred to the respective Fermi level. In the case of zero field, $E_{5s}^{(1,2)}(D, j)$ converges to a constant value for layers j lying sufficiently far away from the interface or the surface (typically two-three unit cells), and the definition of the lineup term is straightforward. Conversely, when the electric field in LAO is nonzero (see Fig. 2), E_{5s} has a linear dependence on the layer index. In particular, deep enough in the film, the variation of E_{5s} between two consecutive cells corresponds precisely to the bulk internal field at the same value of D ,

$$E_{5s}^{(1,2)}(D, j+1) - E_{5s}^{(1,2)}(D, j) = V_{\text{LAO}}(D). \quad (2)$$

Therefore, once $V_{\text{LAO}}(D)$ is known (from the bulk calculations), we can define an *extrapolated* reference energy (see Fig. 2),

$$E_{\text{ref}}^{(1,2)}(D, j) = k(D) + jV_{\text{LAO}}(D), \quad (3)$$

where the constant $k(D)$ is chosen in such a way that $E_{\text{ref}}(D, j) = E_{5s}(D, j)$ far from the interface. Then, we define the lineup term as

$$\phi_{\text{ref}}^{(1,2)}(D) = E_{\text{ref}}^{(1,2)}(D, j_I^{(1,2)}), \quad (4)$$

where $j_I^{(1,2)}$ indicates the interface plane location; here we assume $j_I^{(1)} = 3/4$ and $j_I^{(2)} = 1/4$ (see Fig. 2). Finally, to obtain the n -type SBH $\phi_n^{(1,2)}(D)$ we just need to add to $\phi_{\text{ref}}^{(1,2)}(D)$ the D -dependent band-structure term [we calculate it in the bulk, as the difference between the La(5s) level and the conduction band minimum], $E_{\text{CBM}}(D)$,

$$\phi_n^{(1,2)}(D) = \phi_{\text{ref}}^{(1,2)}(D) + E_{\text{CBM}}(D). \quad (5)$$

Our results for $\phi_n^{(1,2)}(D)$ and $V_{\text{LAO}}(D)$ are shown in Fig. 3(a,b). We find that $\phi_n^{(1,2)}(D)$ behave linearly within the whole studied range. Consequently, the *total* potential drop due to both interfaces can be expressed as $V_I(D) = V_I^0 + C_I^{-1}(D + e/2S)$, where V_I^0 is the total interface potential drop at $D = -e/2S$ and the coefficient C_I^{-1} physically corresponds to the overall inverse interface capacitance density [17, 20]. Considering the potential drop in bulk LAO also to be linear in D [see Fig. 3(b)], i.e. $V_{\text{LAO}}(D) \approx C_b^{-1}(D + e/2S)$, we obtain a simple yet very accurate analytical expression for the electric displacement field in LAO,

$$D(V_{\text{ext}}, N) + \frac{e}{2S} \approx \frac{V_{\text{ext}} - V_I^0}{N C_b^{-1} + C_I^{-1}}, \quad (6)$$

where $C_b^{-1} = 1.36 \text{ m}^2/\text{F}$, $V_I^0 = -0.83 \text{ V}$, and $C_I^{-1} = 1.57 \text{ m}^2/\text{F}$ ($S \equiv a_{\text{STO}}^2$). The inverse bulk LAO capacitance density, C_b^{-1} , is directly related to the static dielectric constant of LAO, $\bar{\epsilon}_{\text{LAO}}$, via $C_b^{-1} = \epsilon_{\text{LAO}} / (\epsilon_0 \bar{\epsilon}_{\text{LAO}})$; in our computational model we have $\bar{\epsilon}_{\text{LAO}} = 31$. For a given value of D , we compute the corresponding electric field using $\mathcal{E}_{\text{LAO}} = (D + e/2S) / \bar{\epsilon}_{\text{LAO}}$. [In the “exact” treatment we replace the average $\bar{\epsilon}_{\text{LAO}}$ with the calculated $\epsilon_{\text{LAO}}(D)$, see the inset of Fig. 3(c)]. Our results for $\mathcal{E}_{\text{LAO}}(V_{\text{ext}}, N)$ are shown in Fig. 3(c). It is worth noting that the outcomes of Eq. (1) [exact, considering non-linearities in $V_{\text{LAO}}(D)$] and Eq. (6) (approximate) are in excellent agreement. In both cases we find that $\mathcal{E}_{\text{LAO}}(V_{\text{ext}}, N)$ monotonically decreases with the inverse of LAO thickness, independently of the applied bias potential.

These results have important implications concerning the interpretation of the experiments reported in Ref. [7]. First, no intrinsic *built-in* LAO electric field exists in the short-circuited Pt/LAO/STO capacitor system, contrary to the assumptions of Singh-Bhalla *et al.* [7]. Second, and most importantly, the uniform decrease of $\mathcal{E}_{\text{LAO}}(V_{\text{ext}}, N)$ with LAO thickness in practice rules out the hypothesis of Zener tunneling that was used in Ref. [7] to explain the abrupt increase of the tunneling current at $N \sim 20$. Indeed, as $\mathcal{E}_{\text{LAO}}(V_{\text{ext}}, N)$ decreases with increasing N , Zener tunneling becomes increasingly less likely in thicker films; note that in our model the LAO valence band *never* goes above the STO Fermi level unless a strong external potential $V_{\text{ext}} \sim 1.8\text{--}1.9 \text{ eV}$ is applied. An alternative interpretation of the aforementioned tunneling experiments

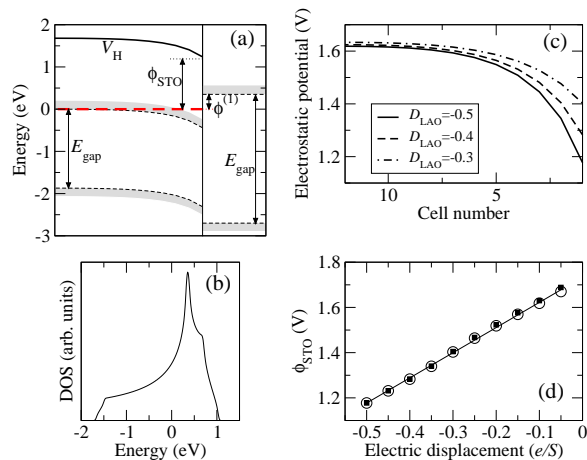


FIG. 4: (a) Mesoscopic band diagram of the LAO/STO junction. The electrostatic potential in STO, V_H , (thick solid curve), the conduction and valence band edges (shaded dashed curves) and the Fermi level (thick dashed line) are shown. (b) Ti t_{2g} density of states of our TB model (V_H is constant and set to zero). (c) V_H as calculated with the TB model (Fermi levels are shifted to zero). (d) Electrostatic potential at the interfacial Ti site as a function of D . Empty circles (filled squares) are calculated for a 12 (24)-layer STO slab and the solid line represents a linear fit to the data.

rests on the results of Ref. [26]. Precisely at a thickness of ~ 20 unit cell, Cancellieri *et al.* reported the onset of in-plane strain relaxation in the LAO overlayer. Such relaxation processes are known to induce defects (e.g. cracks, or misfit dislocations) in the LAO film [26, 27]. It is not unreasonable to think that these defects might constitute preferential paths for electron or hole conduction; also, these defect-mediated conduction processes might explain the hysteretic behavior of the electrical diagrams of Ref. [7]. (The authors invoked the presence of switchable dipoles at the LAO/STO interface, which appears puzzling as neither LAO nor STO are ferroelectric.)

Finally, we shall comment on the microscopic mechanisms that lead to the calculated interface properties. The total interface capacitance density can be expressed as the sum of two contributions,

$$C_I^{-1} = \frac{d}{dD} (\phi_n^{(1)} - \phi_n^{(2)}) = \frac{1}{C^{(1)}} + \frac{1}{C^{(2)}}, \quad (7)$$

each due to a different interface. The variation of $\phi_n^{(2)}(D)$ with D is very small (see Fig. 3); this means that the Pt electrode behaves ideally (“perfect” screening [24]), i.e. $1/C^{(2)} \sim 0$, and therefore we restrict the following analysis to the LAO/STO junction. Specifically, we shall consider the effects of band-bending on $C_{(1)}^{-1}$, i.e. the D -dependent interfacial potential drop that occurs in STO due to the presence of the confined charge carriers [28]. To estimate the band-bending contribution, $\phi_{STO}(D)$, we have employed the tight-binding (TB) model [29] introduced in Ref. [18]. We define $\phi_{STO}(D)$ as the value of

the electrostatic potential in STO at the interfacial Ti site, referred to the Fermi level of the confined electron gas, at a given D [see Fig. 4(a,c)]. Our results show that $\phi_{STO}(D)$ behaves linearly within a wide range of values [Fig. 4(d)]. The band-bending contribution to $C_{(1)}^{-1}$ corresponds to the slope of the linear fit, which amounts to $1.03 \text{ m}^2/\text{F}$. This contribution constitutes a significant fraction (approximately two thirds) of $C_{(1)}^{-1}$. The remainder of $C_{(1)}^{-1}$ is likely to be caused by other effects that typically occur at oxide-oxide interfaces, e.g. intrinsic dielectric “dead layers” [30, 31]. As these appear to be of secondary importance here, we have not pursued this analysis further.

The above results are timely for the interpretation of recent capacitance measurements of thin-film electrode/LAO/STO heterostructures [8]. In the regime of large carrier densities, Li *et al.* measured a dielectric constant of the LAO film of $\epsilon_{LAO} \sim 18$, which is significantly smaller than the typical value reported for LAO single crystals ($\epsilon_{LAO} = 25 - 30$). Our results indicate that this discrepancy may be related to *interfacial* effects, and in particular to the relatively small value of $C^{(1)}$, rather than to the quality of the LAO film. It is worth noting that Li *et al.* [8] used YBCO electrodes, instead of the Pt electrodes considered here. This implies that a possible contribution from the upper electrode interface should be in principle taken into account (recall that $1/C^{(2)}$ essentially vanishes in the present Pt/LAO case) when comparing our data to those of Ref. [8]. In this context, note that Eq. (6) is completely general and applies to any electrode/LAO/STO configuration; one simply needs to replace two parameters (that are specific to the electrode/LAO interface), the Schottky barrier at zero field $\phi_n^{(2)}$ and the interface capacitance $C^{(2)}$. In other words, one does not need to repeat the calculations of the LAO/STO interface, since we have essentially decoupled the bottom from the top electrode and their properties can be computed separately.

In summary, we have studied the electrical properties of metal/LAO/STO capacitors fully from first-principles, determining a complete physical picture of the band offsets and internal fields. Our results and methodologies open new avenues in the first-principles study of functional oxide heterostructures, and provide useful guidelines for the interpretation of the available experimental data on this system.

This work was supported by MICINN-Spain (Grants No. MAT2010-18113 and No. CSD2007-00041), ICREA, and the EC-FP7 project OxIDES (Grant No. CP-FP 228989-2). Computing time was kindly provided by BSC-RES and CESGA.

-
- * Electronic address: mstengel@icmab.es
- [1] A. Ohtomo and H. Y. Wang, *Nature (London)* **427**, 423 (2004).
- [2] S. Thiel *et al.*, *Science* **313**, 1942 (2006).
- [3] Cen *et al.*, *Nature Materials* **7**, 298 (2008).
- [4] W. M. Lü *et al.*, *Appl. Phys. Lett.* **99**, 172103 (2011).
- [5] R. Jany *et al.*, *Appl. Phys. Lett.* **96**, 183504 (2010).
- [6] G. Cheng *et al.*, *Nature Nanotechnology* **6**, 343 (2011).
- [7] G. Singh-Bhalla *et al.*, *Nature Physics* **7**, 80 (2011).
- [8] J. Mannhart and D. G. Schlom, *Science* **327**, 1607 (2010).
- [9] R. Pentcheva and W. E. Pickett, *Phys. Rev. Lett.* **102**, 107602 (2009).
- [10] K. Janicka *et al.*, *Phys. Rev. Lett.* **102**, 106803 (2009).
- [11] P. Delugas *et al.*, *Phys. Rev. Lett.* **106**, 166807 (2011).
- [12] Z. S. Popovic, S. Satpathy, and R. M. Martin, *Phys. Rev. Lett.* **101**, 256801 (2008).
- [13] S. A. Chambers *et al.*, *Phys. Rev. Lett.* **107**, 206802 (2011); L. Qiao *et al.*, *Surface Science* **605**, 1381 (2011).
- [14] H. Chen, A. M. Kolpak, and S. Ismail-Beigi, *Advanced Materials* **22**, 2881 (2010).
- [15] W.-J. Son *et al.*, *Phys. Rev. B* **79**, 245411 (2009).
- [16] N. C. Bristowe, P. B. Littlewood, and E. Artacho, *Phys. Rev. B* **83**, 205405 (2011).
- [17] M. Stengel, N. A. Spaldin, and D. Vanderbilt, *Nature Physics* **5**, 304 (2009).
- [18] M. Stengel, *Phys. Rev. Lett.* **106**, 136803 (2011).
- [19] X. Wu, M. Stengel, K. M. Rabe, and D. Vanderbilt, *Phys. Rev. Lett.* **101**, 087601 (2008).
- [20] M. Stengel, D. Vanderbilt, and N. A. Spaldin, *Nature Materials* **8**, 392 (2009).
- [21] P. E. Blöchl, *Phys. Rev. B* **50**, 17953 (1994)
- [22] We used a plane-wave energy cutoff of 40 Ry and a $6 \times 6 \times 1$ Monkhorst-Pack \mathbf{k} -point grid for Brillouin zone sampling. In the geometry optimizations, atomic forces along the out-of-plane direction were imposed to be smaller than 5 meV/Å .
- [23] The additional charge density is introduced by substituting a cation at the ferroelectric surface by a fictitious cation of different formal valence. As we are interested in exploring intermediate values of D , we generated fictitious pseudopotentials that reproduced fractional nuclear charges.
- [24] M. Stengel *et al.*, *Phys. Rev. B* **83**, 235112 (2011).
- [25] M. Stengel, D. Vanderbilt, and N. A. Spaldin, *Phys. Rev. B* **80**, 224110 (2009).
- [26] C. Cancellieri *et al.*, *Phys. Rev. Lett.* **107**, 056102 (2011).
- [27] Y. Wang, S. G. Kim, and I-W. Chen, *Acta Materialia* **56**, 5312 (2008).
- [28] K. Yoshimatsu *et al.*, *Phys. Rev. Lett.* **101**, 026802 (2008).
- [29] This is based on an electronic t_{2g} -Hamiltonian describing the hoppings between Ti-centered orbitals, wherein the electrical boundary conditions are defined by the electric displacement field in LAO.
- [30] M. Stengel and N. A. Spaldin, *Nature* **443**, 679(2006).
- [31] O. Copie *et al.*, *Phys. Rev. Lett.* **102**, 216804 (2009).